

1 **Evidence of extensive lunar crust formation in impact melt sheets 4330 Myr ago**

2 White, L. F^{1,2*}, Černok, A^{1,2,3}, Darling, J. R⁴, Whitehouse, M.J.⁵, Joy, K. H.⁶, Cayron, C⁷, Dunlop, J⁴,
3 Tait, K. T^{1,2} & Anand, M^{3,8}.

4 ¹*Centre of Applied Planetary Mineralogy, Department of Natural History, Royal Ontario Museum, Toronto,*
5 *Ontario, M5S 2C6, Canada.*

6 ²*Department of Earth Sciences, University of Toronto, Toronto, Ontario, M5S 3B1, Canada.*

7 ³*School of Physical Sciences, The Open University, Milton Keynes, MK7 6AA, UK.*

8 ⁴*School of Earth and Environmental Sciences, Burnaby Building, Burnaby Road, University of Portsmouth,*
9 *Portsmouth, PO1 3QL, UK.*

10 ⁵*Swedish Museum of Natural History, Box 50007, SE-104 05 Stockholm, Sweden*

11 ⁶*School of Earth and Environmental Science, University of Manchester, Oxford Road, Manchester, M13 9PL,*
12 *UK.*

13 ⁷*Laboratory of ThermoMechanical Metallurgy (LMTM), École Polytechnique Fédérale de Lausanne (EPFL),*
14 *Rue de la Maladière 71b, 2000 Neuchâtel, Switzerland.*

15 ⁸*Department of Earth Sciences, The Natural History Museum, Cromwell Road, London, SW7 5BD, UK.*

16 **Corresponding author: lwhite@rom.on.ca*

17

18 **Accurately constraining the formation and evolution of the lunar magnesian (Mg) suite**
19 **is key to understanding the earliest periods of magmatic crustal building that followed**
20 **accretion and primordial differentiation of the Moon. However, the origin and evolution**
21 **of these unique rocks is highly debated. Here, we report on the microstructural**
22 **characterisation of a large (~250 µm) baddeleyite (monoclinic-ZrO₂) grain in Apollo**
23 **troctolite 76535 that preserves quantifiable crystallographic relationships indicative of**
24 **reversion from a precursor cubic-ZrO₂ phase. This observation places important**
25 **constraints on the formation temperature of the grain (> 2300 °C) which endogenic**
26 **processes alone fail to reconcile. We conclude that the troctolite crystallized directly**
27 **from a large, differentiated impact melt sheet 4326 ± 14 million years (Myr) ago. These**
28 **results suggest that impact bombardment would have played a critical role in the**
29 **evolution of the earliest planetary crusts.**

30 Insights into the formation, differentiation and impact bombardment of planetary
31 bodies have been derived through geodynamic modelling, remote sensing observations, and
32 isotopic analysis of planetary meteorites and returned samples. The resulting models are
33 hindered by the paucity of mineralogical evidence that can place direct constraints on these
34 very high temperature and pressure processes. Although many mineral thermobarometers can
35 record geological temperatures ranging up to a maximum of ~1500 °C, empirical
36 mineralogical and geochemical evidence of higher temperatures is often lost due to extensive

37 recrystallization and melting (and melt loss) at such conditions. Recently, microstructural
38 analysis of the accessory mineral baddeleyite has revealed new insights into the high-
39 temperature history of shock-melted rocks¹, with grains preserving microstructural evidence
40 of high-temperature and high-pressure ZrO₂ polymorphs despite reversion to the stable
41 monoclinic structure at ambient conditions. For example, tracing the phase heritage of
42 baddeleyite disassociated from zircon to the cubic-ZrO₂ structure has constrained peak
43 temperature conditions of a terrestrial impact melt to > 2370 °C at ambient surface
44 pressures^{1,2} (Figure 1), far in excess of that attainable with traditional mineral
45 geothermometers¹. Previous reports of cubic-ZrO₂ phase heritage are restricted to grains
46 found in relatively young terrestrial rocks, such as ~37.8 Ma grains from the Mistastin Lake
47 impact structure (Canada)^{1,3}. As such, the ability for individual baddeleyite grains to preserve
48 the rich microstructural heritage required to conduct phase reconstruction analysis across
49 planetary timescales (over four billion years) is currently less established, though zirconia
50 phase heritage has the potential to yield new insights into the high pressure and temperature
51 history of Solar System processes^{1,4}. Here, we undertake geochemical and microstructural
52 analyses on an exceptional baddeleyite grain in a sample of the lunar Mg-suite, which reveals
53 the diagnostic crystallographic relationships indicative of cubic-ZrO₂ phase heritage. This
54 observation places new constraints on the mechanisms involved in lunar crustal evolution.

55 Lunar troctolite 76535, sampled by the Apollo 17 mission, is one of the most
56 intensively studied samples from the Moon⁵⁻⁷. An unshocked, coarse-grained example of the
57 Mg-suite, petrological observations suggest 76535 likely crystallized at a depth of 10 to 30
58 km within the lunar crust⁸ before ejection and transportation to the Apollo sampling sites,
59 potentially from as far afield as the South Pole Aitken basin⁹. This low-shock state is
60 common among samples collected by the Apollo astronauts, with only ~1% of materials
61 containing maskelynite, a diaplectic glass of feldspar composition only formed at high
62 pressure (> 28 GPa)¹⁰. The rock has been considered chemically pristine (i.e. endogenously
63 igneous) principally due to low abundances of highly siderophile elements¹¹, however Os-
64 isotope ratios provide evidence for minor meteoritic contamination¹². The Mg-suite as a
65 whole preserves contradictory chemical signatures, with high Mg/(Mg+Fe) ratios, indicative
66 of more primitive reservoirs, contrasting with high rare earth element signatures of their
67 parent melts suggestive of an evolved magmatic source^{6,13,14}. Reconciling these observations
68 has proved challenging¹⁵, and still represents a major area of uncertainty for lunar scientists
69 that invokes a mantle overturn hypothesis¹⁴. The chronology of the studied sample has been

70 intensively investigated, yielding a ^{147}Sm - ^{143}Nd age of $4307 \pm 11 \text{ Myr}^7$, a Rb-Sr age of 4279
71 $\pm 52 \text{ Myr}^7$, and an ^{40}Ar - ^{39}Ar age of $4249 \pm 12 \text{ Myr}^{16}$, which collectively define a cooling rate
72 of $3.9^\circ\text{C} / \text{Myr}^7$. Following exhumation at 4249 Myr , as defined by the low temperature Ar-
73 Ar chronometer, there is no evidence for further heating events above $\sim 400^\circ\text{C}$.

74 Within the analysed section (thin section ,51), a large ($80 \times 250 \mu\text{m}$) subhedral
75 baddeleyite crystal displays several distinctive crystallographic domains (each 2 to $50 \mu\text{m}$ in
76 width) that are clearly observable at the resolution of optical microscopy (Figure 2a). No
77 amorphous or crystalline silica (SiO_2) was observed in direct contact with the analysed
78 baddeleyite grain, suggesting the phase does not represent a product of high-temperature
79 dissociation from a zircon (ZrSiO_4) precursor¹⁷ and instead remained pure ZrO_2 throughout
80 its formation and evolution. Electron microprobe analysis (EMPA) of the grain reveals 1.26
81 wt% TiO_2 and 1.4 wt% HfO_2 (all EPMA data are reported in the supplementary materials),
82 while other impurities (Mg, Ca, Fe, Al, and Si) constitute $< 0.08 \text{ wt}\%$ each in total. Dating of
83 the grain using secondary ion mass spectrometry (SIMS) reveals a spread of $^{207}\text{Pb}/^{206}\text{Pb}$ dates
84 between $4334.5 \pm 4.6 \text{ Myr}$ (2σ uncertainty) and $4311.3 \pm 6.7 \text{ Myr}$, yielding high scatter on
85 the calculated weighted average age of $4326 \pm 16 \text{ Ma}$ (2 standard deviation uncertainty). The
86 grain is between 40 and 63 million years older than previously reported ages from smaller
87 baddeleyite grains within the same rock ($4271 \pm 29 \text{ Myr}^5$). Detailed analysis of the grain
88 using electron backscatter diffraction (EBSD) techniques facilitated the quantification of the
89 variant orientations (Figure 2b), revealing a range of unique disorientation relationships
90 between the domains: predominately $90^\circ/\langle 001 \rangle$, $180^\circ/\langle 001 \rangle$, and $180^\circ/\langle 9,0,10 \rangle$. Reduction
91 of the entire EBSD dataset using the ARPGE¹⁸ software package highlights peaks in
92 disorientation analysis at 90° , 120° and 180° which, along with the presence of three unique
93 crystallographic axes in the $\langle 010 \rangle$ (*b*-axis) direction along three $\langle 100 \rangle$ cubic directions
94 (Figure 2c), cannot be explained by reversion from the tetragonal or orthorhombic systems
95 alone^{1,2,4}. However, the phase heritage of the grain can be confidently associated with
96 reversion from a single cubic- ZrO_2 precursor (Figure 2d).

97 Formative temperatures for cubic- ZrO_2 vary based on the major and trace element
98 composition of the ZrO_2 grain. Although the influence of TiO_2 and HfO_2 on the P-T-t
99 conditions required to induce high symmetary ZrO_2 polymorphs is unconstrained, oxide
100 impurities typically have to occur in concentrations on the order of $\sim 10 \text{ wt}\%$ to substantially
101 influence phase transformation temperatures within the ZrO_2 system¹⁹. The temperature
102 required to induce the cubic- ZrO_2 phase also varies based on the confining pressure of the

103 annealed sample¹, while the influence of oxygen fugacity on the transition is currently
104 unknown. However, at ~30 km depth (as estimated for the maximum formation depth of
105 76535⁸), an estimated ~0.2 GPa of confining pressure would facilitate formation of cubic-
106 ZrO₂ at ~2300 °C.

107 Thermal models of the Moon cannot reconcile these required temperatures through
108 endogenic processes alone²⁰, although impact-induced melting of crustal rocks has been
109 modelled to generate sufficient temperatures (~2300 °C) as to facilitate cubic-ZrO₂
110 formation¹. While this previous occurrence of cubic phase heritage is reported from within
111 impact melt generated by a small (28 km) impact structure (Mistatin Lake), it is reasonable to
112 assume that larger melt sheets would reach comparable temperature conditions. Large impact
113 melt sheets are widely reported from the Moon, with recent studies into the formation of the
114 South Pole-Aitken basin suggesting that the impactor generated a 50 km deep melt pool²¹. An
115 event similar to this magnitude would be more than sufficient to produce the deep, super-
116 heated impact melt sheet required to produce both a coarse-grained assortment of
117 differentiated mafic rocks²² and the high temperature cubic-ZrO₂ polymorph. It should be
118 noted that while sufficiently elevated temperatures would also be attained during the Moon-
119 forming impact itself²³, this event occurred up to 200 Myr ago, prior to the genesis of the
120 76535 troctolite²⁴. In addition to these chronological constraints, modelling of the event
121 suggests ~100 % of the particles accreted into the lunar body would have reached
122 temperatures in excess of 5000°C²³. Significantly in excess of the temperature required to
123 melt and vaporize ZrO₂¹⁷, the Moon forming impact would lead to a complete loss of phase
124 heritage¹, and as such we move forward on the assumption that the Moon-forming impact
125 cannot have been responsible for the formation of the cubic ZrO₂ polymorph.

126 Although the crystallization potential of baddeleyite is directly controlled by the
127 oxygen fugacity and Zr content of the parent magma, in all scenarios it is one of the last
128 phases to crystallize out of a melt²⁵. Thus, it is unlikely that a super-heated impact melt sheet
129 would solidify cubic-ZrO₂ directly unless unrealistically oversaturated in Zr (notably, this has
130 not been reported from large terrestrial impacts). Baddeleyite crystallizing directly from a
131 cooling impact melt would be expected to form at lower temperatures (< 1000 °C) and, thus,
132 not contain the interlocking reversion structures indicative of high-temperature phase
133 heritage. This suggests that our analysed baddeleyite grain crystallized as *m*-ZrO₂ within a
134 primordially differentiated precursor material (likely KREEP enriched) prior to incorporation
135 into the impact melt, whereby the elevated magmatic temperatures induced transformation to

136 the *c*-ZrO₂ structure (>2300 °C; Figure 1). This observation does not contradict the potential
137 overturn of a lunar magma ocean¹⁴, which could also explain the incorporation of a KREEP-
138 rich layer into the impact melt environment. Given that disturbance of the U-Pb isotope
139 system within the baddeleyite grain likely occurred during both phase transition²⁶ and
140 subsequent annealing²⁷ it is assumed that the oldest Pb-Pb age recorded by the grain (4334.1
141 ± 4.2 Ma) represents the age of reversion from the high-temperature cubic-ZrO₂ structure.
142 The 34 million year spread of Pb-Pb ages (4299.5 ± 8.8 to 4334.1 ± 4.2 Ma) supports this
143 observation (Figure 3), hinting at staggered resetting of the U-Pb systematics during
144 incorporation into the impact melt sheet. Fresh baddeleyite growth likely occurred at 4271 ±
145 29 Ma (based on previous dating of significantly smaller baddeleyite⁵) during the final
146 crystallization stages of troctolite 76535 as supported by the observed age overlap with whole
147 rock Ar-Ar chronometry¹⁶. Importantly, our new Pb-Pb data are concordant with two impact
148 grown zircons recovered from a breccia containing clasts of shocked Mg-suite norite and
149 impact melt (Apollo 15 sample 15455) that record ages of 4332 ± 6 Ma and 4326 ± 10 Myr
150 ²⁸. These zircon grains contain remnant baddeleyite cores, and are interpreted as
151 recrystallizing and dissociating during an impact event (whereby the ZrSiO₄ grains separate
152 to the constituent oxides ZrO₂ and SiO₂ above ~1650 °C¹⁷). Coupled with our new temporal
153 and temperature constraints from coarse grained troctolite 76535, these observations provide
154 an argument for the generation of a large, super-heated impact meltsheet at ~4330 Myr ago,
155 for which the Mg-suite appears to retain robust crystallographic and isotopic evidence.

156 Our findings provide new insights into the potential formation mechanisms for the
157 earliest secondary lunar crust. Measurement of ²⁰⁷Pb-²⁰⁶Pb ages of baddeleyite and zircon,
158 along with refractory ¹⁴⁷Sm-¹⁴³Nd and ¹⁴⁶Sm-¹⁴²Nd isotope systematics suggest that the
159 ferroan anorthosite (FAN) suite of rocks formed as young as 4360 ± 3 Ma²⁹, supporting either
160 a young Moon (which is problematic given the oldest lunar zircon, dated at 4417 ± 6 Ma³⁰) or
161 formation of early lunar crust through non magma ocean processes. Here, the discovery of
162 the high temperature (≥ 2300 °C) cubic-ZrO₂ polymorph in Apollo 17 troctolite 76535
163 suggests that large differentiated impact melt sheets could provide a mechanism for crustal
164 formation immediately after lunar magma ocean crystallization, either in conjunction with or
165 instead of rejuvenated or serial endogenic magmatism. This discovery supports
166 interpretations of the Sr and Nd isotope systematics of FAN sample 60025 and Mg-suite
167 sample 76535 which imply that both the FAN and Mg-suite crystallised from magmatic
168 reservoirs that became isolated almost immediately before the crystallization of the rocks⁷.

169 Although these Sr and Nd isotope systematics could also be explained by minimal
170 differentiation of the bulk Moon⁷, variations in major and trace element composition of the
171 Mg-suite rocks support rapid formation and isolation of source magmas. This rapid
172 generation of distinct source magmas for the FAN and Mg-suite could be facilitated by
173 impact bombardment, with insulated melt sheets encouraging the localised slow cooling and
174 differentiation of Mg-suite rocks. Any siderophile element signature inherited from the
175 meteoritic impactor could be diluted and heterogeneously distributed throughout the large
176 impact melt sheet³¹, and thus measured abundances would vary throughout the resultant
177 lithologies. In addition, at least one large impact around 4330 Myr ago would account for the
178 preponderance of Sm-Nd and Lu-Hf model ages around this time³², as well as an observed
179 peak in zircon U-Pb ages²⁸. Super-heated impact-induced melt sheets provide an alternative
180 and, based on our new crystallographic and chronological evidence, more likely explanation
181 for this observed clustering of ages.

182 Though a differentiated impact-melt sheet origin was previously proposed for the Mg-
183 suite troctolites in the early 1990's³³, this model has been generally disregarded by more
184 recent studies¹⁴. However, our new temperature and temporal constraints strongly suggest
185 that at least one key sample from the Mg-suite, which records contradictory chemical
186 signatures of primitive and evolved sources that are challenging to reconcile with endogenic
187 lunar processes alone¹⁵, originated from a super-heated impact melt sheet which likely
188 homogenised varying quantities of primordially differentiated crustal suites. Though the melt
189 sheet would likely have undergone differentiation and fractional crystallization³⁴, the isotopic
190 and elemental composition of this melt is largely dependent on that of the target lithologies³⁵,
191 suggesting incorporation of an underlying urKREEP component into the melt source of
192 troctolite 76535. Such interactions would produce the conflicting chemical signatures and
193 variable compositions observed in other samples from the Mg-suite, whilst retaining the
194 'pristine' siderophile elemental signature ascribed to the suite¹². Thus, we suggest that the
195 impact-melt sheet hypothesis likely explains the origin of at least some members of the
196 enigmatic Mg-suite. On a larger scale, our findings provide strong evidence for at least one,
197 though potentially multiple, large-scale bombardment events in the early history of the Moon
198 (≥ 4330 Myr ago), suggesting that the evolution of evolved planetary crusts around this time
199 is intrinsically linked to impact events. Given the timing of this bombardment, it is possible
200 that early impacts into a differentiating Moon may have provided the melting and mixing
201 required to initiate overturn of lunar magma ocean cumulates around 4350 Myr ago. Such

202 impacts would also satisfy previous predictions that ancient basaltic magmatism (recently
203 dated to 4370 - 4340 Myr ago³⁶) would be triggered by large basin forming events³⁷. Such
204 evidence has previously remained concealed in the lunar rock record.

205 Although this study represents the sole report of prior cubic-ZrO₂ within a lunar
206 sample, the implications of this discovery for crustal formation on the Moon should re-
207 invigorate detailed investigations of existing and future returned lunar samples. Meteoritic
208 baddeleyite are often highly deformed, and as such the discrete crystallographic structures
209 incorporated into this phase heritage approach could be partially overprinted during shock
210 ejection from the lunar surface. As such, the preservation potential of these features in
211 meteoritic samples is currently unknown. Our discovery of cubic-ZrO₂ phase heritage in
212 ancient (~4330 million years old) baddeleyite grains pushes back the preservation age of
213 these crystallographic structures by ~4300 million years¹⁷, revealing the robustness of
214 microstructural phase heritage across the timescales required to probe the early Solar System.
215 This crystallography-driven approach can thus be applied to a wide range of baddeleyite-
216 bearing planetary lithologies in an effort to improve our understanding of early, high-
217 temperature Solar System processes by directly interpreting the rock record of these planet-
218 shaping events.

219

220 **Main References**

- 221 1. Timms, N. E. *et al.* Cubic zirconia in >2370 °C impact melt records Earth's hottest
222 crust. *Earth Planet. Sci. Lett.* **477**, 52–58 (2017).
- 223 2. Cayron, C., Douillard, T., Sibil, A., Fantozzi, G. & Sao-Jao, S. Reconstruction of the
224 cubic and tetragonal parent grains from electron backscatter diffraction maps of
225 monoclinic zirconia. *J. Am. Ceram. Soc.* **93**, 2541–2544 (2010).
- 226 3. Sylvester, P., Crowley, J. & Schmitz, M. U-Pb zircon age of Mistastin Lake crater,
227 Labrador, Canada - implications for high-precision dating of small impact melt sheets
228 and the end Eocene extinction. in *Mineralogical Magazine* 2295 (2013).
- 229 4. White, L. F. *et al.* Baddeleyite as a widespread and sensitive indicator of meteorite
230 bombardment in planetary crusts. *Geology* **46**, 719–722 (2018).
- 231 5. Hinthorne, J. R., Conrad, R. & Andersen, C. A. Lead-lead age and trace element
232 abundances in lunar troctolite 76535. in *Lunar and Planetary Science Conference*
233 *Proceedings.* (1975).
- 234 6. Elrado, S. M., McCubbin, F. M. & Shearer Jr, C. K. Chromite symplectite in Mg-suite
235 troctolite 76535 as evidence for infiltration metasomatism of a lunar layered intrusion.

- 236 *Geochim. Cosmochim. Acta* **87**, 154–177 (2012).
- 237 7. Borg, L. E., Connelly, J. N., Cassata, W. S., Gaffney, A. M. & Bizzarro, M.
238 Chronological implications for slow cooling of troctolite 76535 and temporal
239 relationships between the Mg-suite and the ferroan anorthosite suite. *Geochim.*
240 *Cosmochim. Acta* **201**, 377–391 (2017).
- 241 8. Gooley, R., Brett, R., Warner, J. & Smyth, J. . A lunar rock of deep crustal origin:
242 sample 76535. *Geochim. Cosmochim. Acta* **38**, 1329–1339 (1974).
- 243 9. Garrick-Bethell, I. *et al.* Troctolite 76535: A sample of the Moon’s South Pole-Aitken
244 basin? *Icarus* **338**, (2020).
- 245 10. Rubin, A. E. Maskelynite in asteroidal, lunar and planetary basaltic meteorites: An
246 indicator of shock pressure during impact ejection from their parent bodies. *Icarus*
247 **257**, 221–229 (2015).
- 248 11. Warren, P. H. A concise compilation of petrologic information on possibly pristine
249 nonmare Moon rocks. *Am. Mineral.* **78**, 360–376 (1993).
- 250 12. Day, J. M. D., Walker, R. J., James, O. B. & Puchtel, I. S. Osmium isotope and highly
251 siderophile element systematics of the lunar crust. *Earth Planet. Sci. Lett.* **289**, 595–
252 605 (2010).
- 253 13. Elrado, S. M., Draper, D. S. & Shearer Jr, C. K. Lunar Magma Ocean crystallization
254 revisited: Bulk composition, early cumulate mineralogy, and the source regions of the
255 highlands Mg-suite. *Geochim. Cosmochim. Acta* **75**, 3024–3045 (2011).
- 256 14. Shearer, C. K., Elrado, S. M., Petro, N. E., Borg, L. E. & McCubbin, F. M. Origin of
257 the lunar highlands Mg-Suite: An integrated petrology, geochemistry, chronology, and
258 remote sensing perspective. *Am. Mineral.* **100**, 294–325 (2015).
- 259 15. Taylor, S. R., Norman, M. D. & Esat, T. M. The Mg-suite and the highland crust: An
260 unsolved enigma. in *Proceedings of the Lunar and Planetary Science Conference Vol.*
261 *24* (1993).
- 262 16. Garrick-Bethell, I., Weiss, B. P., Shuster, D. L., Tikoo, S. M. & Tremblay, M. M.
263 Further evidence for early lunar magnetism from troctolite 76535. *J. Geophys. Res.*
264 *Planets* **121**, 1–18 (2016).
- 265 17. Timms, N. E. *et al.* A pressure-temperature phase diagram for zircon at extreme
266 conditions. *Earth-Science Rev.* **165**, 185–202 (2017).
- 267 18. Cayron, C. ARPGE: a computer program to automatically reconstruct the parent grains
268 from electron backscatter diffraction data. *J. Appl. Crystallogr.* **40**, 1183–1188 (2007).
- 269 19. Swab, J. *Role of Oxide Additives in Stabilizing Zirconia for Coating Applications.*

- 270 (2001).
- 271 20. Zhang, N., Parmentier, E. M. & Liang, Y. A 3-D numerical study of the thermal
272 evolution of the Moon after cumulate mantle overturn: The importance of rheology
273 and core solidification. *J. Geophys. Res. Planets* **118**, 1789–1804 (2013).
- 274 21. Hurwitz, D. M. & Kring, D. A. Differentiation of the South Pole-Aitken basin impact
275 melt sheet: Implications for lunar exploration. *J. Geophys. Res. Planets* **119**, 1110–
276 1133 (2014).
- 277 22. Latypov, R., Chistyakova, S., Grieve, R. & Huhma, H. Evidence for igneous
278 differentiation in Sudbury Igneous Complex and impact-driven evolution. *Nat.*
279 *Commun.* 1–13 (2019). doi:10.1038/s41467-019-08467-9
- 280 23. Canup, R. M. & Asphaug, E. Origin of the Moon in a giant impact near the end of the
281 Earth’s formation. *Nature* **412**, 708–712 (2001).
- 282 24. Jacobson, S. A. *et al.* Highly Siderophile Elements in the Earth’s Mantle as a Clock for
283 the Moon-forming Impact. *Nature* **508**, 84–87 (2014).
- 284 25. Herd, C. D. K. *et al.* in *Microstructural Geochronology: Planetary Records Down to*
285 *Atom Scale* (eds. Moser, D. E., Corfu, F., Darling, J. R., Reddy, S. M. & Tait, K.) 137–
286 165 (American Geophysical Union, 2018).
- 287 26. White, L. F. *et al.* Atomic scale age resolution of planetary events. *Nat. Commun.*
288 (2017). doi:10.1038/ncomms15597
- 289 27. Darling, J. R. *et al.* Variable microstructural response of baddeleyite to shock
290 metamorphism in young basaltic shergottite NWA 5298 and improved U–Pb dating of
291 Solar System events. *Earth Planet. Sci. Lett.* **444**, 1–12 (2016).
- 292 28. Crow, C. A., McKeegan, K. D. & Moser, D. E. Coordinated U–Pb geochronology,
293 trace element, Ti-in-zircon thermometry and microstructural analysis of Apollo
294 zircons. *Geochim. Cosmochim. Acta* **202**, 264–284 (2017).
- 295 29. Borg, L. E., Connelly, J. N., Boyet, M. & Carlson, R. W. Chronological evidence that
296 the Moon is either young or did not have a global magma ocean. *Nature* **477**, 70–72
297 (2011).
- 298 30. Nemchin, A. *et al.* Timing of crystallization of the lunar magma ocean constrained by
299 the oldest zircon. *Nat. Geosci* **2**, 133–136 (2009).
- 300 31. Petrus, J. A., Ames, D. E. & Kamber, B. S. On the track of the elusive Sudbury
301 impact: geochemical evidence for a chondrite or comet bolide. *Terra Nov.* **27**, 9–20
302 (2015).
- 303 32. Borg, L. E., Gaffney, A. M. & Shearer, C. K. A review of lunar chronology revealing a

- 304 preponderance of 4.34-4.37 Ga ages. *Meteorit. Planet. Sci.* **50**, 715–732 (2015).
- 305 33. Hess, P. C. The petrogenesis of lunar troctolites. *J. Geophys. Res.* **99**, 19083–19093
306 (1994).
- 307 34. O’Connell-Cooper, C. D. & Spray, J. G. Geochemistry of the impact-generated melt
308 sheet at Manicouagan: Evidence for fractional crystallization. *J. Geophys. Res. Solid
309 Earth* **116**, B6 (2011).
- 310 35. Darling, K. R., Hawkesworth, C. J., Storey, C. D. & Lightfoot, P. C. Shallow impact:
311 Isotopic insights into crustal contributions to the Sudbury impact melt sheet. *Geochim.
312 Cosmochim. Acta* **74**, 5680–5696 (2010).
- 313 36. Snape, J. F. *et al.* Ancient volcanism on the Moon: Insights from Pb isotopes in the
314 MIL 13317 and Kalahari 009 lunar meteorites. *Earth Planet. Sci. Lett.* **502**, 84–95
315 (2018).
- 316 37. Elkins-Tanton, L. T., Hager, B. H. & Grove, T. L. Magmatic effects of the lunar late
317 heavy bombardment. *Earth Planet. Sci. Lett.* **222**, 17–27 (2004).
- 318 38. Park, J. *et al.* Newly determined Ar/Ar ages of lunar troctolite 76535. in *Proceedings
319 of the 46th Lunar and Planetary Science Conference* (2015).
- 320 39. Heaman, L. M. & LeCheminant, A. N. Paragenesis and U-Pb systematics of
321 baddeleyite (ZrO_2). *Chem. Geol.* **110**, 95–126 (1993).
- 322 40. Marchi, S. *et al.* High-velocity collisions from the lunar cataclysm recorded in
323 asteroidal meteorites. *Nat. Geosci.* **6**, 303–307 (2013).
- 324 41. Hiesinger, H. *et al.* New crater counts of the South Pole-Aitken basin. in *EGU General
325 Assembly* 8410 (2012).

326

327 **Acknowledgments**

328 L.F.W and A.C are funded by a Hatch postdoctoral fellowship. A.C. has received
329 funding from the European Union's Horizon 2020 research and innovation programme under
330 grant agreement No-704696 RESOLVE, and M.A’s contribution to this work was partly
331 funded by the UK Science and Technology Facilities Council (ST/L000776/1 &
332 ST/P000657/1). The NordSIMS facility is supported by Swedish Research Council
333 infrastructure grant no. 2017-00671 and the Swedish Museum of Natural History; this is
334 NordSIMS publication no. 609. K.H.J acknowledges STFC grant ST/M001253 and Royal
335 Society grant UF140190. J.R.D acknowledges STFC grant ST/S000291/1 and Royal Society
336 Research Grant RG160237. We thank Geoff Long for conducting colloidal silica polishing of

337 the thin section to facilitate EBSD analysis of the target grain. M.A. thanks NASA CAPTEM
338 for the allocation of polished thin section 76535,51.

339

340 **Author Contributions**

341 L.F.W., A.C., J.R.D. and M.A. designed the initial study. L.F.W., A.C., J.R.D. and
342 J.D. conducted electron backscatter diffraction analysis of the baddeleyite grain. C.C.
343 conducted phase reconstruction using the ARPGE and GenOVa software packages. A.C. and
344 M.W conducted SIMS analysis on the baddeleyite grain. All authors discussed the results and
345 interpretation, and commented on the manuscript at all stages.

346

347 **Author Information**

348 Reprints and permissions information is available at www.nature.com/reprints. The
349 authors declare no competing financial interests. Readers are welcome to comment on the
350 online version of the paper. Correspondence and requests for materials should be addressed
351 to L.F.W (lwhite@rom.on.ca).

352

353 **Competing Interests**

354 The authors declare no competing interests.

355

356 **Methods**

357 All work was conducted *in situ* within a thin-section that was vibratory polished with
358 0.05 micron alumina. The target baddeleyite grain was located in section 76535,51 using
359 traditional microscopy techniques, and backscatter electron (BSE) images were collected
360 using a Zeiss EVO MA10 LaB₆ scanning electron microscope (SEM) housed at the
361 University of Portsmouth. Micro- to nano-scale structural analysis was conducted by electron
362 backscatter diffraction (EBSD) using an Oxford Instruments Nordlys EBSD detector
363 mounted on the same SEM instrument. No coating was applied, and EBSD analyses were
364 performed under variable pressure conditions, using N₂ to neutralize charging. The sample
365 was tilted at 70° within the chamber at a working distance of 14 mm, before analysis using an
366 electron beam with an accelerating voltage of 20 kV and a probe current of 1 nA. The grain
367 was mapped using the AZTEC software package (Oxford instruments), which facilitates
368 automated collection of kikuchi diffraction patterns from set spatial intervals. The grain was
369 initially mapped at 1 μm step size to confirm the presence of complex microstructure

370 suggested by petrological imaging of the grain. To collect a more robust dataset, the grain
371 was reanalyzed at 500 nm step size, to more fully capture smaller crystallographic domains.
372 The complete map yielded 53,038 indexed baddeleyite data points. Monoclinic-ZrO₂ was
373 indexed using ref [42], and although crystallographic cards for orthorhombic-ZrO₂, tetragonal-
374 ZrO₂ and cubic-ZrO₂ were included during analysis the phases were never indexed by the
375 software. Wild spike reduction was completed on all EBSD datasets, although no other form
376 of raw data correction (i.e. infilling of zero solutions) was conducted.

377 Reconstruction of all indexed baddeleyite reveals a single cubic parent grain which
378 can be attributed to the generation of all monoclinic orientations in the measured dataset
379 (Supplementary Figure 1). Analysis of the entire EBSD dataset using the ARPGE¹⁸ software
380 package highlights peaks in disorientation analysis at 90°, 120° and 180° which can be
381 associated with cubic to monoclinic reversion of the grain. These disorientations closely
382 match those predicted by Type 2 orientation relationships (OR) ((100)_m//(100)_c &
383 [010]_m//[010]_c)², matching those observed in impact melt samples at Mistastin Lake¹
384 (Supplementary Figure 2a). This observation is further strengthened by the presence of three
385 unique crystallographic axes in the <010> (*b*-axis) direction along the three <100> cubic
386 directions of the prior cubic grain, as shown by the stereographic pole figures of the <100>,
387 <010> and <001> directions and their simulations made with the software GenOVA⁴³ in
388 Supplementary Figure 2b,c which cannot be explained by reversion from the tetragonal or
389 orthorhombic systems alone².

390 The pole figures of the planes are reported in Supplementary Figure 2b, whereby the
391 comparison between the experimental and simulated pole figures also shows that Type 1 OR
392 exists besides the major Type 2 OR. This additional OR explains the peaks at 80° and 115° in
393 the disorientation histogram (Supplementary Figure 2a). To localize the intermediate
394 tetragonal domains, the 12 monoclinic variants inherited from the cubic grains were
395 partitioned into three packets of four variants sharing the same *b*-axis oriented along the same
396 <100> *c*-axis (Supplementary Figure 2d). The analysis reveals that one *b*-packet dominates
397 the two other ones, which proves that a majority (but not all) the baddeleyite grains come
398 from a unique prior tetragonal domain (in blue in Supplementary Figure 2d) crossed by a
399 second large tetragonal domain (in red) and smaller third domains (in green). Only a single,
400 cubic parent can explain the microstructure observed here.

401 The thin-section was coated with ~30 nm layer of gold on the top of the carbon coat,
402 to reduce gold accumulation in the cracks. Pb- isotopic measurements of baddeleyite were

403 performed using a CAMECA IMS1280 ion microprobe at the NordSIMS facility, Swedish
404 Museum of Natural History (Stockholm), closely following previously reported protocols^{36,44}.
405 The Hyperion H201 RF plasma source was used to generate a 23kV impact energy, 2.5 nA,
406 Gaussian focussed primary beam of O₂⁻ ions, which was used together with an in-run raster of
407 5 μm to yield a spot of ca 8 μm diameter. Oxygen flooding of the sample chamber was used
408 to enhance secondary Pb ion yields from baddelyite by a factor of 7. Secondary Pb⁺ ions were
409 mass filtered at M/ΔM of 4860 and detected simultaneously in four low-noise ion-counting
410 electron multipliers. Detector gains were calibrated using BCR-2g basaltic glass and common
411 Pb corrected ²⁰⁷Pb/²⁰⁶Pb ratios were further normalised to bracketing analyses (n = 6) of
412 Phalaborwa baddelyite (2060.6 Ma⁴⁵). Data reduction was performed using an in-house
413 developed software at NordSIMS. The ²⁰⁷Pb/²⁰⁶Pb ages assume the decay constants
414 recommendations of Steiger and Jäger (1975) and are reported with 2σ errors. The effects of
415 common lead on the measured ²⁰⁷Pb/²⁰⁶Pb ages were calculated using a variety of modelled
416 scenarios, from terrestrial contamination to variable influence of lead from lunar basalt and
417 KREEP terranes. In all cases, the measured age is only altered by < 0.8 Ma (Supplementary
418 Table 4), minimising the risk of common lead resulting in the older than published values for
419 baddeleyite in troctolite 76535.

420

421 **Data Availability**

422 The authors declare that data supporting the findings in this study are available within
423 the paper and its Supplementary Information files. All other data are available from the
424 corresponding author upon request.

425

426 **Additional References**

- 427 42. Smith, D. K. & Newkirk, W. The crystal structure of baddeleyite (monoclinic ZrO₂)
428 and its relation to the polymorphism of ZrO₂. *Acta Crystallogr.* **18**, 983–991 (1965).
- 429 43. Cayron, C. GenOVA: a computer program to generate orientational variations. *J. Appl.*
430 *Crystallogr.* **40**, 1179–1182 (2007).
- 431 44. Whitehouse, M. J., Kamber, D. S., Fedo, C. M. & Lepland, A. The importance of
432 combined Pb and S isotope data from early Archaean rocks, southwest Greenland, for
433 the interpretation of S-isotope signatures. *Chem. Geol.* **222**, 112–131 (2005).
- 434 45. Reischmann, T. Precise U/Pb age determination with baddeleyite (ZrO₂), a case study
435 from the Phalaborwa igneous complex, South Africa. *South African J. Geol.* **98**, 1–4
436 (1995).

437
438
439
440
441
442
443
444
445
446
447
448
449
450
451
452
453
454
455
456
457
458
459
460
461
462
463
464
465
466
467
468
469
470
471
472
473
474
475
476
477
478

Supplementary Information is available in the online version of the paper.

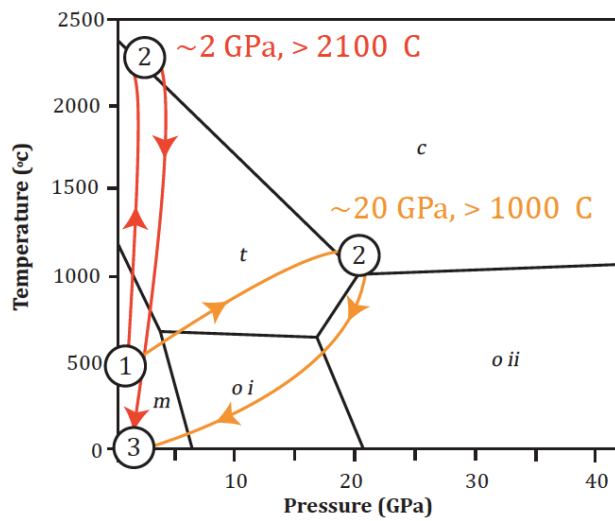


Figure 1: Phase diagram of the ZrO₂ system. Stable at ambient conditions, monoclinic-ZrO₂ (1) transitions to the meta-stable tetragonal-ZrO₂ (t) and cubic-ZrO₂ (c) structure at high temperature conditions (2) before reverting to m-ZrO₂ upon cooling (3). At high pressures, grains will transform through a series of orthorhombic-ZrO₂ polymorphs (o i and o ii). While the exact temperature required to induce the cubic structure varies based on confining pressure (e.g. red versus orange P-T pathways), if high pressure conditions were reached shock effects associated with > 20 GPa of loading would be observed in the troctolite. The pristine nature of troctolite 76535 suggests no such shock pressures were experienced, supporting origin by a super-heated melt. This supports a formation temperature of at least 2300 °C for the cubic ZrO₂ structure, which cannot be attained by endogenic processes alone. (Adapted from ref¹⁷).

479
480
481
482
483
484
485
486
487
488
489
490
491
492
493
494
495
496
497
498
499
500
501
502
503
504
505
506
507
508
509
510
511
512
513
514
515
516
517
518
519
520
521

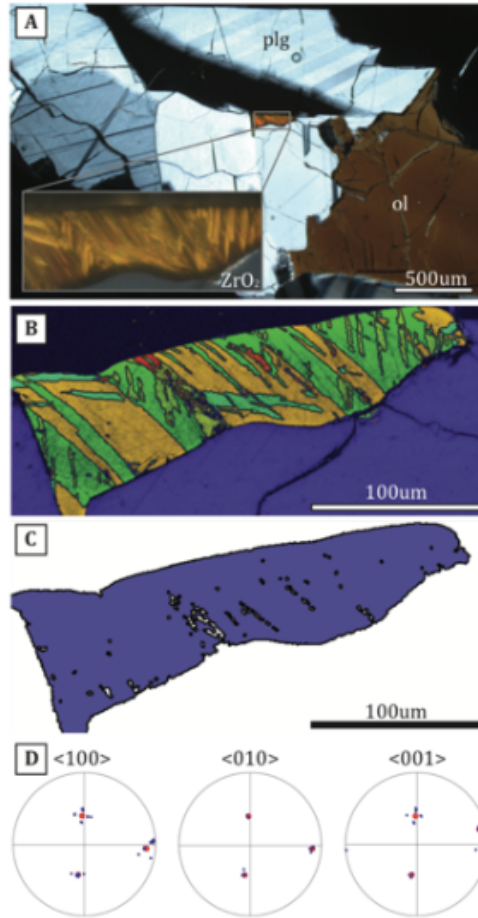


Figure 2: Optical imaging, EBSD data and parent grain reconstruction for the large baddeleyite grain in Apollo sample 76535. Cross polarized light (XPL) overview of the target grain, highlighting the crystalline and unshocked nature of the surrounding plagioclase (plg) and olivine (ol) (A). Inset image of target baddeleyite (ZrO₂) grain highlights the density and complexity of twin relationships observable even at low optical resolution (40x magnification). EBSD data reveal an abundance of monoclinic domains throughout the grain, with colour coded mapping of crystallographic orientations (enhanced from inverse pole figure) revealing structural complexity within the grain (B). Reconstruction of these measured domains using the ARPGE software package¹⁸ is conducted by quantifying each monoclinic orientation before tracing relationships back to a single cubic precursor grain, as shown in (C). This process is aided by the disorientation relationships observed in <100>, <010> and <001> directional pole figures of the dataset (D), which reveal the correlation between measured baddeleyite orientations (blue data) and the calculated orientation of cubic precursors (red data). A small number of pixels could not be reconstructed in this manner, potentially representing neoblastic overgrowth during further annealing.

522
 523
 524
 525
 526
 527
 528
 529
 530
 531
 532
 533
 534
 535
 536
 537
 538
 539
 540
 541
 542
 543
 544
 545
 546
 547
 548
 549
 550
 551
 552
 553
 554
 555

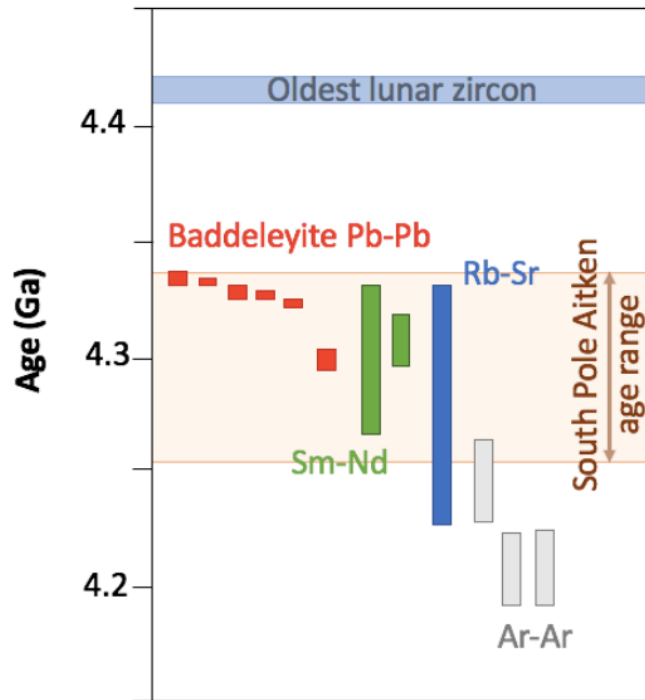


Figure 3: Pb-Pb data generated by SIMS analysis of the large reversion twinned baddeleyite grain in troctolite 76535, and comparison to published Sm-Nd⁷, Rb-Sr⁷ and Ar-Ar³⁸ chronology for the same rock. The mean squared weighted deviation of 13 suggests the ages record excess scatter, providing evidence that the spread of ages (between 4299.5 ± 4.4 Ma and 4334.1 ± 2.1 Ma) is real and not analytical. This partial age resetting on the grain scale is indicative of Pb loss induced during phase reversion, where the rapid heating and cooling associated with the impact melt sheet fail to completely homogenise the U-Pb systematics²⁶. Importantly, our Pb isotope data define the age of Pb diffusion in baddeleyite (> 950 °C³⁹), comparable to the previously described cooling rate⁷. Generated baddeleyite ages fall within previously defined age estimates for both the FAN and Mg suites of lunar rocks. For reference, ages of the oldest measured lunar zircon³⁰ and the estimated age of the South Pole Aitken basin^{40,41}, which has been modelled to be a potential source terrane⁹, are also presented.